Transcriptomic Stratification of Late-Onset Alzheimer's Cases Reveals Novel Genetic Modifiers of Disease Pathology

Nikhil Milind[1,2*], Christoph Preuss[1*], Annat Haber[1], Guru Ananda[1], Shubhabrata Mukherjee[3], Cai John[1], Sarah Shapley[1,4], Anna L. Tyler[1], Benjamin A. Logsdon[5], Paul K. Crane[3], Gregory W. Carter[1†]

*These authors contributed equally to this work.

[1]The Jackson Laboratory, Bar Harbor, ME, USA 04609

[2]Program in Genetics, Department of Biological Science, North Carolina State University, Raleigh, NC, USA 27695

[3]Department of Medicine, School of Medicine, University of Washington, Seattle, WA, USA 98195

[4]Program in Neuroscience, Department of Biology & Geology, Baldwin Wallace University, Berea, OH, USA 44017

[5]Sage Bionetworks, Seattle, WA, USA 98121

Keywords: Alzheimer' disease, gene expression, co-expression modules, reproducibility

†Correspondence:
Gregory Carter, Ph.D.
The Jackson Laboratory
600 Main Street
04609 Bar Harbor, Maine
Phone: (207)288-6025
Email: Gregory.Carter@jax.org

ABSTRACT

Late-Onset Alzheimer's disease (LOAD) is a common, complex genetic disorder well-known for its heterogeneous pathology. The genetic heterogeneity underlying common complex diseases poses a major challenge for targeted therapies and the identification of novel disease-associated variants. Case-control approaches are often limited to examining a specific outcome in a group of heterogenous patients with different clinical characteristics. Here, we developed a novel approach to define relevant transcriptomic endophenotypes and stratify decedents based on molecular profiles in three independent human LOAD cohorts. By integrating post-mortem brain gene co-expression data from 2114 human samples with LOAD, we developed a novel quantitative, composite phenotype that can better account for the heterogeneity in genetic architecture underlying the disease. We used iterative weighted gene co-expression network analysis (WGCNA) analysis to reduce data dimensionality and to isolate gene sets that are highly co-expressed within disease subtypes and represent specific molecular pathways. We then performed single variant association testing using whole genome-sequencing data for the novel composite phenotype in order to identify genetic loci that contribute to disease heterogeneity. Distinct LOAD subtypes were identified for all three study cohorts (two in ROSMAP, three in Mayo Clinic, two in Mount Sinai Brain Bank). Single variant association analysis identified a genome-wide significant variant in *TMEM106B* (p-value < 5×10^{-8}, rs1990620^{G}) in the ROSMAP cohort that confers protection from the inflammatory LOAD subtype. Taken together, our novel approach can be used to stratify LOAD into distinct molecular subtypes based on affected disease pathways.

INTRODUCTION

Late-onset Alzheimer's disease (LOAD) is the most common form of dementia in the elderly. The clinical features associated with LOAD are an amnesic type of memory impairment, deterioration of language, and visuospatial deficits. In the later stages of the disease, symptoms may include motor and sensory abnormalities, gait disturbances, and seizures. Without advances in therapy, the number of symptomatic cases in the United States is predicted to rise to 13.2 million by 2050[1].

Many common, complex diseases such as LOAD present with heterogeneous phenotypes due to interactions between genetic and environmental factors affecting a range of pathways and processes. LOAD has no simple form of inheritance and is governed by a common set of risk alleles across multiple genes that, in combination, have a substantial effect on disease predisposition and age of onset[2]. Genome-Wide Association Studies (GWAS) have become an important tool for identifying variants in complex diseases[3,4]. GWAS for LOAD have identified variants in over 500 genes as potential risk factors with the ε4 variant in *APOE* as the strongest contributor to overall disease risk[2,5]. LOAD has a strong polygenic component and an estimated heritability of up to 80%[6]. It has been challenging to transition from the identification of associated genetic variants to the molecular mechanisms that lead to the accumulation of amyloid plaques and helical tau filaments[7]. Furthermore, there is mounting evidence that the observed heterogeneity in LOAD is associated with multiple distinct subtypes[8,9].

Gene co-expression modules tend to consist of genes that belong to the same cellular pathways or programs and help explain the global properties of the transcriptome as it

relates to disease risk[10]. Networks-based co-expression module approaches have been used to identify causal variants in Late-Onset Alzheimer's disease[7,11]. However, such studies have failed to account for the heterogeneity of mechanisms that lead to complex diseases. Here, we analyze whole genome sequencing (WGS) and whole transcriptome data from three independent human cohorts from the Accelerating Medicines Partnership - Alzheimer's Disease (AMP-AD) Consortium. We use gene co-expression modules to develop quantitative phenotypes that account for the complex genetic architecture and heterogeneity of LOAD to more effectively map associated variants using genome-wide assocation. Furthermore, the method presented in this paper can be used to identify variants in other complex diseases.

METHODS

Whole genome sequencing and RNA sequencing data

We obtained whole-genome sequencing and RNA sequencing (RNA-Seq) data from Synapse (https://www.synapse.org/) for three cohorts from the AMP-AD consortium, from the Mayo Clinic, Mount Sinai Brain Bank, and Rush University. The Mayo Clinic (Mayo) cohort consists of 276 temporal cortex (TCX) samples from 312 North American Caucasian subjects consisting of cases characterized with LOAD, pathological aging (PA), progressive supranuclear palsy (PSP), or elderly controls[12] (Synapse:syn5550404). The Mount Sinai Brain Bank (MSBB) cohort consists of 214 frontopolar prefrontal cortex (FP), 187 inferior temporal gyrus (IFG), 160 parahippocampal gyrus (PHG), and 187 superior temporal gyrus (STG) samples characterized with LOAD, elderly control, or mild cognitive impairment (MCI) (Synapse: syn3159438). The Rush University's Religious Orders Study and Memory and Aging Project (ROSMAP) cohort consists of 623 dorsolateral prefrontal cortex (DLPFC)

samples of individuals from 40 groups of religious orders from across the United States (ROS) and older adults in retirement communities in the Chicago area (MAP), characterized with LOAD, elderly control, or MCI[7,13] (Synapse:syn3219045). A summary of samples from each of the cohorts is provided in Table S1 and Table S2. Sex, age of death, and batch were used as covariates for normalization in the ROSMAP and Mayo data. Sex, age of death, race, and batch were used as covariates for normalization in the MSBB data. Details on post-mortem brain sample collection, tissue and RNA preparation, sequencing, and sample quality control can be found in published work related to each cohort[12,14,15].

Co-expression modules and iterativeWGCNA

Data on human AMP-AD co-expression modules were obtained from Synapse (Synapse: syn11932957.1). The modules derive from the three independent LOAD cohorts used in this study. A detailed description on how co-expression modules were identified can be found in a recent study that identified the human co-expression modules as part of a transcriptome wide LOAD meta-analysis[16]. In brief, a modified procedure using five different co-expression analysis protocols followed by merging by graph clustering methods was performed to obtain 30 modules across all three cohorts (Synapse: syn2580853), 26 of which corresponded to the six tissue regions used in this study. A summary of these modules is provided in Table S3. We focused on tissues from the frontal cortex, temporal cortex, and hippocampus due to their relevance to LOAD neuropathology[17]. These modules are generally large, containing thousands of genes that represent multiple functions[16]. In order to construct more functionally-specific submodules from these AMP-AD co-expression modules, we subjected them to a repeated pruning process called iterativeWGCNA[18]. Briefly, iterativeWGCNA performed WGCNA on each AMP-AD co-expression module independently. The gene sets produced by this process were then

pruned to ensure that only highly correlated genes remained by evaluating the connectivity of the genes to the gene set eigengene. The resulting gene sets, containing highly correlated genes, were combined and the process was repeated until the gene sets converged. The algorithm then attempted to reclassify genes from the residual gene set. We specified a soft-threshold power of six, a minimum eigengene connectivity of 0.6, and a required module size of 100 to promote the generation of submodules that capture pathway-level signals. The final set of 68 submodules consisted of highly correlated and cell-type specific genes. The submodules were mutually exclusive for a given cohort but overlapped with submodules from other cohorts. A summary of these submodules is provided in Table S4. An eigengene for a given submodule is defined as the first principle component of gene expression data within each submodule.

Stratification of LOAD cases based on clustering of human co-expression submodules

Eigengene expression data for TCX, PHG, FP, and DLPFC regions was used to stratify LOAD cases in separate analyses. Clustering was performed on submodule eigengenes to determine subtypes of LOAD cases in each brain region. The NbClust R package determined the optimal number of clusters for different clustering methods by polling with the majority rule across 30 indices[19]. We tested agglomerative hierarchical approaches (Ward, UPGMA, WPGMA) and a reallocation approach (K-means) on the eigengene expression data and evaluated the within-cluster similarity of cases using silhouettes. The silhouette for a given object is a measure that simultaneously assesses how similar the object is to its cluster and how different the object is from all the other clusters[20]. Prior analysis of simulated genome-wide methylation data suggests that no one clustering method outperforms the other consistently and that mean silhouette widths can be used to

158 pick the ideal clustering method[21]. The silhouette plots revealed that different methods were
159 required for the different regions to generate clusters with the largest average silhouette
160 widths. We determined that K-means was an optimal approach for DLPFC, Ward was
161 optimal for PHG and TCX, and UPGMA was optimal for FP after analyzing silhouette plots
162 of clusters generated by each method for each region. An example of silhouettes used to
163 determine the ideal clustering method for the DLPFC region is shown in Figure S1. A
164 summary of the clusters for each brain region, considered case subtypes, is provided in
165 Table S5. In the subtypes generated for the DLPFC region from the ROSMAP cohort, we
166 assessed each subtype for enrichment of cognitive and pathological measures. We used
167 Braak stages as a measure of neurofibrillary tangle burden and CERAD scores as a
168 measure of neuritic plaque burden[22,23]. We also assessed the rate of decline in memory,
169 executive function, visuospatial function, and language across the subtypes. Definitions,
170 collection, and standardization of these decline measures can be found in previously
171 published work[24].
172
173 **Differential expression analysis of case subtypes**
174 For differential expression analysis, control decedents were defined as cognitively-normal
175 and MCI decedents for PHG, FP, and DLPFC. In the case of TCX, control decedents were
176 defined as cognitively normal, PSP, and PA decedents. For each of the regions used to
177 stratify LOAD cases (TCX, PHG, FP, and DLPFC), we performed differential expression
178 analysis to compare gene expression in case subtypes with control decedents as described
179 above. We used the limma R package to perform the differential expression analysis
180 between subtype and control decedents[25]. We used the clusterProfiler R package to
181 perform KEGG and Reactome pathway analysis on differentially expressed genes to
182 determine the signal captured by clustering on eigengene expression data[26].

183

184 **Single-variant association of eigengene expression and subtype specificity**

185 We used EMMAX, a variance component linear mixed model, to perform single-variant
186 association of our newly derived quantitative traits[27]. Each submodule eigengene was used
187 as a quantitative trait in single-variant association for its respective brain region. For each
188 region, we also developed a subtype specificity metric by calculating the Euclidean
189 distance between the eigengene expression profile of each decedent and the centroid of
190 each subtype cluster. This resulted in a vector of scores for each subtype that was mapped
191 separately. All quantitative trait mapping results had a genomic inflation factor near one,
192 indicating that there was no significant population substructure effect on the mapping. QQ
193 plot analysis on the p-values showed no evidence of population substructure or
194 confounding effects (Figure S2).

195

196 **Replication of suggestive and significant SNPs in other cohorts**

197 The ROSMAP cohort represented the most adequately powered cohort in the study and
198 was used as a baseline for assessing replication of suggestive and significant SNPs in the
199 other cohorts. SNPs were considered suggestive if quantitative trait mapping with either the
200 submodule eigengenes or the subtype specificity metric resulted in a p-value smaller than
201 1×10^{-5} and genome-wide significant if they resulted in a p-value smaller than 5×10^{-8}, which
202 are standard cutoffs for GWAS. Suggestive and significant SNPs from the DLPFC region in
203 ROSMAP were considered replicated in the TCX, FP, and PHG regions if the SNPs were
204 associated with the submodule eigengenes or subtype specificity metric of the given region
205 at a p-value of 0.05. Summary statistics of prior association studies were obtained from the
206 NHGRI-EBI catalog[28]. Loci were considered replicated if suggestive and significant SNPs
207 from the ROSMAP cohort were reported in these studies at a p-value smaller than 5×10^{-8}.

A summary of the entire analysis is provided in Figure S3.

RESULTS

Refinement of 26 human co-expression modules identifies disease-associated transcriptomic signals

We performed an iterative gene list pruning process using the iterativeWGCNA approach to refine the 26 human co-expression modules from the AMP-AD consortium. This resulted in subsets, or submodules, of highly correlated genes that were exclusive to each module. Genes that were not highly correlated to any submodule were removed since they are less likely to contribute to the overall signal of the submodule and more likely to introduce noise. We compared the submodules and detected specific LOAD-associated molecular pathways and processes that are shared across the three post-mortem brain cohorts and six brain regions (Figure S4). Furthermore, incorporating information from previously defined cell-type specific markers derived from bulk RNA-Seq and single cell RNA-Seq[29] showed that pruning the 26 co-expression modules into 68 submodules resulted in multiple novel cell-type specific submodules (Figure 2, Figure S5). Taken together, these novel 68 submodules reflect 15 specific functional consensus clusters that are associated with distinct pathways and processes related to LOAD (Figure S4).

Submodule gene sets capture biological signals specific to LOAD pathology

We annotated submodules using GO term enrichment, KEGG pathway enrichment, and Reactome pathway enrichment to highlight the biological specificity of co-expression signals captured by the different submodules (Table S6, Table S7, Table S8). While the 26 harmonized co-expression modules were associated with five distinct consensus clusters

that captured a broader signal, the submodule associations were more specific in terms of functional enrichment (Figure S4). The 15 functional consensus clusters associated with the 68 submodules revealed cell-type specific signatures and elucidated gene sets for specific biological pathways, including tau-protein kinase activity, neuroinflammation, myelination, and cytoskeletal reorganization (Figure S4).

Single-variant association mapping of submodule eigengenes

To map the genetic drivers of biological disease-associated signals resolved by submodules, we performed single-variant association mapping of submodule eigengenes. Eigengenes were defined as the first principle component of the gene expression data associated with each submodule. They capture the variation of gene co-expression and reduce noise associated with the transcriptomic data. Genome-wide suggestive and significant loci were detected for submodules in all four brain regions (Table S9, Table S10, Table S11, Table S12). We identified multiple loci that were replicated across the cohorts at a genome-wide significant level. For instance, rs1990620 is a known variant in *TMEM106B* that was identified as genome-wide significant in the DLPFC region from the ROSMAP cohort was replicated ($p < 5\times10^{-2}$) in all other brain regions from the Mayo and MSSM cohorts.

Stratification of LOAD cases based on 68 AMP-AD co-expression submodules

Clustering LOAD cases in subtypes based on eigengenes provided a method of assessing genetic drivers of heterogeneity in the transcriptome of LOAD cases. The NbClust package chose between two and three clusters for each region and the number of cases in each cluster was balanced (Table S5). The subtypes were not enriched for common LOAD-associated covariates, such as sex, *APOEε4* genotype, or years of education (Figure 4).

Eigengene expression profiles for each subtype were used to assess the association of each subtype with molecular and biological pathways associated with submodules. An example for the ROSMAP cohort is shown in Figure 4. We observed no significant enrichment of cognitive or neuropathological measures between the subtypes for the DLPFC region (Figure S6).

ROSMAP subtypes differ in inflammatory response

In order to better understand the underlying molecular differences across the novel LOAD associated subtypes in the ROSMAP cohort and to identify potential subtype specific candidate markers, differential expression analysis was performed for each of the previously defined subtypes against a set of controls (Figure 5a). Each of the two subtypes was compared to a set of 471 decedents from the ROSMAP cohort that were either cognitively normal or had mild cognitive impairment. The Venn diagram in Figure 5b depicts the comparison across the different subtypes. Interestingly, cases associated with Subtype A showed a stronger transcriptional response with 127 differentially expressed genes (adjusted p-values < 0.05, absolute log fold change > 0.5) when compared with controls. Of these genes, 86 were up-regulated and 41 were down-regulated. Among the most significantly down-regulated genes associated with Subtype A cases was the stress-response mediator corticotropin-releasing hormone (*CRH*). Overacting *CRH* signaling has been implicated in inflammatory disorders and LOAD where it has been proposed as a therapeutic target to reduce the negative effects of chronic stress related to memory function and amyloid beta (Aβ) production[30]. Cases associated with Subtype B had 40 differentially expressed genes (adjusted p-values < 0.05, absolute log fold change > 0.5), 39 of which were down-regulated when compared to controls. Notably, two key pro-inflammatory mediators of amyloid deposition (*S100A8, S100A9*) were among the most

283 significantly down-regulated genes in Subtype B decedents when compared to controls
284 (Figure 5a). Both genes, which are established inflammatory biomarkers, are part of a
285 complex that serves as a critical link between the amyloid cascade and inflammatory
286 events in LOAD[31]. Furthermore, multiple pathways linked to *S100A8/9* activation, including
287 IL-10 signaling and complement activation were enriched across down-regulated genes in
288 Subtype B but not in Subtype A decedents as highlighted in Figure 5c. In addition,
289 molecular pathways linked to microglia activation (Figure S8), the immune response, and
290 the stress response were found among the most significant pathways and gene sets (Table
291 S13, Table S14) that differ across subtypes. Gene set enrichment analysis revealed a
292 subset of genes linked to the KEGG osteoclast differentiation pathway (Figure S8),
293 including known AD risk markers such as *TREM2*, *TYROBP*, and *CCL2* among others
294 which were highly up-regulated in Subtype A cases compared to Subtype B cases. This
295 highlights that both molecularly defined LOAD subtypes differ in their immune response
296 and that known LOAD biomarkers, including *S100A8/A9*[32], *TREM2,* and *CCL2* might be
297 used to stratify patients based upon their inflammatory response to the observed disease
298 state. These results were consistent with the functional annotations of the previously
299 defined submodules that define both subtypes (Figure 4C).
300
301 **Single variant association mapping for ROSMAP decedents**
302 Genome wide association mapping revealed a differential enrichment of significant variants
303 across subtypes (Figure 6, Table S9, Table S10, Table S11, Table S12). Loci were
304 associated with one or more submodule eigengenes, as shown in Figure 6. One genome-
305 wide suggestive allele in *TMEM106B* was identified for Subtype B (p-value < 4×10^{-6},
306 rs1990620^{G}). This association was replicated at a genome-wide suggestive level in
307 association with the DLPFCbrown_2 eigengene and at a genome-wide significant level with

the DLPFCbrown_1 and DLPFCyellow_2 eigengenes (Figure 3). DLPFCbrown_1 contains genes related to myelination and lysosomal activity (KEGG pathways hsa00600 and hsa04142), while DLPFCyellow_2 contains genes related to endocytosis and potassium channel activity (KEGG pathway hsa04144 and Reactome pathway R-HSA-1296071). *TMEM106B* is a known modifier of neurodegenerative disease and cognitive aging, which has been previously linked with cognitive performance[33]. Loss of *TMEM106B* function has been shown to rescue lysosomal phenotypes related to frontotemporal dementia[34]. The identified protective allele rs1990620^{G} is a known CCCTC-binding factor (CTCF) site, which has been shown to modify the inflammatory response in the course of aging[35]. Besides the association with *TMEM106B* in Subtype B, protective variants near *MTUS2* were identified which are in close vicinity to *HMGB1*, a locus that has been previously implicated in brain atrophy[36]. A differential expression analysis of haplotype carriers of the protective rs1990620^{G} variant in *TMEM106B* showed an up-regulation of neuroactive ligand receptor interactions, while decedents carrying the risk variant showed significant up-regulation for pathways related to Osteoclast differentiation (KEGG pathway hsa04380) and neuroinflammation (data not shown).

Suggestive SNPs in ROSMAP are replicated in other cohorts

A total of 1326 unique SNPs representing 163 loci were genome-wide suggestive or significant (p-value < 1×10^{-5}) in the DLPFC region when pooled from all 11 DLPFC eigengenes and two subtype-specific variant mapping analyses. Of these, 645 SNPs were replicated in the PHG analyses, 762 SNPs were replicated in the FP analysis, and 482 SNPs were replicated in the TCX analyses (p-value < 1×10^{-2}). The *TMEM106B* variant associated with dementia, rs1990620, was replicated in all cohorts. Of the 163 loci, 29 loci

across 27 studies had been previously reported in the NHGRI-EBI catalog such that the most significant SNP from the prior study was a suggestive SNP in the DLPFC region (Table S15, Table S16, Table S17, Table S18).

DISCUSSION

Common complex diseases such as LOAD are characterized by phenotypic heterogeneity and the presence of multiple common variants affecting disease risk. In this study, we present an analysis that uses transcriptomic co-expression data and whole-genome sequencing from multiple cohorts to dissect phenotypic heterogeneity and identify potential genetic drivers of complex trait pathology in LOAD.

Here, we used an iterative pruning approach based on 26 human post-mortem co-expression modules to generate 68 novel submodules that contained genes associated with LOAD specific biological pathways and molecular processes. Indeed, we observed that genes in the novel submodules are enriched for functional terms that were specific to pathways associated with LOAD, such as lipid modification, the TREM2/TYROBP pathway, and tau-protein kinase activity. Furthermore, submodules from all six brain regions clustered independently of the co-expression module of origin and brain region, suggesting that the genes captured in each submodule represented signals that were associated with LOAD pathology rather than cohort- or tissue-specific factors. Notably, submodules were much more specific for markers of different brain cell types, suggesting that the processes associated with submodules represent the pathological signals from these specific cell types. This is in line with recent studies showing that different cell types in the brain play specific roles at different stages in the pathogenesis of LOAD[37]. Taken together, our results

357 demonstrate that the novel human co-expression submodules identified in this study
358 capture cell-type specific pathways associated with LOAD pathogenesis in the brain.
359
360 Mapping the eigengene expression for individual submodules represents a pathway- or
361 process-level alternative to expression quantitative trait locus (eQTL) mapping for each
362 individual transcript. Since the human co-expression submodules represented pathological,
363 cell-type specific pathways in LOAD brain tissue, mapping eigengene expression for
364 decedents was expected to identify genetic drivers of LOAD pathology. RNA-Seq data from
365 post-mortem brain tissue in human cohorts contains a strong immune signal, as evidenced
366 by repeated identification of genetic loci related to microglial response in meta-analyses
367 with increasingly large cohorts[5,38]. Using submodule eigengenes as quantitative traits for
368 single-variant association provided an opportunity to identify genetic drivers of biological
369 processes that are known to be drivers of early LOAD pathogenesis, such as astrogliosis,
370 neuronal plasticity, myelination, and vascular blood brain barrier interactions[37]. Suggestive
371 variants identified were unique to subsets of submodules. For instance, the *TMEM106B*
372 locus was associated at a genome-wide significant level with the DLPFCbrown_1 and
373 DLPFCyellow_2 eigengenes (Figure 3), representing processes related to oligodendrocytic
374 myelination, lysosomal activity, endocytosis, and potassium channel activity. The
375 *TMEM106B* locus has been implicated in cognitive aging, with functional consequences in
376 frontotemporal dementia related to lysosomal activity[33–35]. A submodule of particular
377 interest is the microglia-associated submodule DLPFCblue_3, which contains genes
378 related to the TREM2/TYROBP cascade. The *FAM110A* locus is close to rs1014897 and
379 the *CNTNAP5* locus is close to rs76854344, both variants have been previously associated
380 with posterior cortical atrophy and LOAD[39]. The *NTM* locus is close to rs1040103, a variant
381 that has been associated with white blood cell count[40]. Thus, quantitative trait mapping of

single variants using eigengene expression for submodules presented in this study can elucidate genetic factors specific to associated pathological pathways.

Furthermore, eigengenes represent a dimensional reduction of transcriptomic data onto axes of pathological relevance. Thus, we expected that clustering on the eigengene expression of LOAD cases would generate pathway-level profiles of putative molecular LOAD subtypes based on case heterogeneity. As anticipated, we observed that average eigengene expression was enriched by subtype for multiple submodules in all four brain regions tested. Strikingly, these enrichments were diametric in the subtypes generated for LOAD cases, an example of which is presented for the DLPFC region in Figure 4. Similar enrichment patterns were identified in the other three brain regions. These results suggest that the biological programs identified by submodules in this study align themselves along the heterogeneity of transcriptomic data present in LOAD cases across multiple cohorts rather than differentiating solely based on cases and controls. Furthermore, the stratification of patients based on submodule expression profiles demonstrated that there is significant variation in immune response in post-mortem brain tissue, a process that is considered a hallmark of LOAD pathogenesis (Figure 5, Figure S8). Variants associated with the subtype specificity metric overlapped with the variants associated with individual submodule eigengenes (Figure 6). This suggests that the genetic factors that influenced subtypes can be dissected into loci driving specific submodules. Furthermore, the deconstruction of genetic loci can provide the basis for more targeted treatment of dysfunctional pathways that contribute to different subtypes of LOAD.

Our subtypes in the DLPFC brain region of the ROSMAP cohort represent differences in transcriptomic profiles of LOAD cases derived from post-mortem RNA-Seq data. A lack of

temporal data makes it challenging to decisively interpret these profiles. The subtypes may represent distinct LOAD endpoints, differences in disease severity, environmental effects, or phases of molecular pathology. Neither subtype was associated with cognitive or neuropathological outcome (Figure S6). Furthermore, covariates such as sex, *APOE* genotype, and years of education were not significantly enriched in any given subtype (Figure 4). This suggests that the transcriptomic profiles do not represent transitions in disease severity and that there are overall risk factors not reflected in transcriptomic subtypes. Furthermore, both subtypes are associated with unique loci that belong to the same community of loci detected by submodule mapping (Figure 6), indicating that the subtypes capture various combinations of genetic elements that lead to LOAD pathology. While suggestive, these transcriptomic LOAD subtypes will require further validation in cohorts that adequately control for disease progression.

The methodology presented in this study is not limited to RNA-Seq data and can be performed on other omics, such as proteomics or metabolomics. As such data become available for the decedents in these cohorts, this analysis can be expanded across these additional informative dimensions.

ACKNOWLEDGEMENTS

This study was supported by the National Institutes of Health grant U54 AG 054354. Additional funding was provided by the Barbara H. Sanford Endowed Scholarship Fund, the Robert E. Garrity Cooperative Education Fund as well as the Park and Goldwater Scholarship funds. We thank A. Saykin and K. Nho for helpful conversations.

The results published here are in whole or in part based on data obtained from the AMP-AD Knowledge Portal (doi:10.7303/syn2580853). Study data were provided by the Rush Alzheimer's Disease Center, Rush University Medical Center, Chicago. Data collection was supported through funding by NIA grants P30AG10161, R01AG15819, R01AG17917, R01AG30146, R01AG36836, U01AG32984, U01AG46152, the Illinois Department of Public Health, and the Translational Genomics Research Institute.

The results published here are in whole or in part based on data obtained from the AMP-AD Knowledge Portal (doi:10.7303/syn2580853). Study data were provided by the following sources: The Mayo Clinic Alzheimer's Disease Genetic Studies, led by Dr. Nilufer Taner and Dr. Steven G. Younkin, Mayo Clinic, Jacksonville, FL using samples from the Mayo Clinic Study of Aging, the Mayo Clinic Alzheimer's Disease Research Center, and the Mayo Clinic Brain Bank. Data collection was supported through funding by NIA grants P50 AG016574, R01 AG032990, U01 AG046139, R01 AG018023, U01 AG006576, U01 AG006786, R01 AG025711, R01 AG017216, R01 AG003949, NINDS grant R01 NS080820, CurePSP Foundation, and support from Mayo Foundation. Study data includes samples collected through the Sun Health Research Institute Brain and Body Donation Program of Sun City, Arizona. The Brain and Body Donation Program is supported by the National Institute of Neurological Disorders and Stroke (U24 NS072026 National Brain and Tissue Resource for Parkinson's Disease and Related Disorders), the National Institute on Aging (P30 AG19610 Arizona Alzheimer's Disease Core Center), the Arizona Department of Health Services (contract 211002, Arizona Alzheimer's Research Center), the Arizona Biomedical Research Commission (contracts 4001, 0011, 05-901 and 1001 to the Arizona Parkinson's Disease Consortium) and the Michael J. Fox Foundation for Parkinson's Research. The results published here are in whole or in part based on data obtained from

the AMP-AD Knowledge Portal (doi:10.7303/syn2580853). These data were generated from postmortem brain tissue collected through the Mount Sinai VA Medical Center Brain Bank and were provided by Dr. Eric Schadt from Mount Sinai School of Medicine.

AUTHOR'S CONTRIBUTIONS

NM, CP, AH, GA and CJ performed the genetic and transcriptomic analysis. SS annotated the functional variants. SM and PC provided cognitive and phenotype data for the analysis. BL and AT provided additional transcriptomic data for the analysis. GWC supervised and designed the project. NM, CP and GWC wrote the manuscript. All authors read and approved the final manuscript.

CONSENT FOR PUBLICATION

All authors have approved of the manuscript and agree with its submission.

COMPETING INTERESTS

Not applicable.

REFERENCES

1. Cummings, J. L. Alzheimer's Disease. *N. Engl. J. Med.* **351,** 56–67 (2004).
2. Bertram, L. & Tanzi, R. E. Thirty years of Alzheimer's disease genetics: the implications of systematic meta-analyses. *Nat. Rev. Neurosci.* **9,** 768–778 (2008).
3. Kilpinen, H. & Barrett, J. C. How next-generation sequencing is transforming complex disease genetics. *Trends Genet.* **29,** 23–30 (2013).
4. Risch, N. & Merikangas, K. The future of genetic studies of complex human diseases. *Science* (1996). doi:10.1126/science.273.5281.1516
5. Jansen, I. E. *et al.* Genome-wide meta-analysis identifies new loci and functional pathways influencing Alzheimer's disease risk. *Nat. Genet.* **51,** 404–413 (2019).
6. Verheijen, J. & Sleegers, K. Understanding Alzheimer Disease at the Interface between Genetics and Transcriptomics. *Trends Genet.* **34,** 434–447 (2018).
7. Mostafavi, S. *et al.* A molecular network of the aging human brain provides insights into the pathology and cognitive decline of Alzheimer's disease. *Nat. Neurosci.* **21,** 811–819 (2018).
8. Mukherjee, S. *et al.* Genetic data and cognitively-defined late-onset Alzheimer's disease subgroups. *Mol. Psychiatry* 1–10 (2018). doi:10.1101/367615
9. Ferreira, D. *et al.* Distinct subtypes of Alzheimer's disease based on patterns of brain atrophy: longitudinal trajectories and clinical applications. *Sci. Rep.* **7,** 1–13 (2017).
10. Langfelder, P. & Horvath, S. Eigengene networks for studying the relationships between co-expression modules. *BMC Syst. Biol.* **1,** 54 (2007).
11. Zhang, B. *et al.* Integrated systems approach identifies genetic nodes and networks in late-onset Alzheimer's disease. *Cell* **153,** 707–20 (2013).
12. Allen, M. *et al.* Human whole genome genotype and transcriptome data for

Alzheimer's and other neurodegenerative diseases. *Sci. Data* **3,** (2016).

13. Chibnik, L. B. *et al.* Susceptibility to neurofibrillary tangles: role of the PTPRD locus and limited pleiotropy with other neuropathologies. *Mol. Psychiatry* **23,** 1521–1529 (2018).

14. Wang, M. *et al.* The Mount Sinai cohort of large-scale genomic, transcriptomic and proteomic data in Alzheimer's disease. *Sci. Data* **5,** 1–16 (2018).

15. De Jager, P. L. *et al.* A multi-omic atlas of the human frontal cortex for aging and Alzheimer's disease research. *Sci. Data* **5,** 1–13 (2018).

16. Logsdon, B. *et al.* Meta-analysis of the human brain transcriptome identifies heterogeneity across human AD coexpression modules robust to sample collection and methodological approach. *bioRxiv* 510420 (2019). doi:10.1101/510420

17. DeTure, M. A. & Dickson, D. W. The neuropathological diagnosis of Alzheimer disease. *Mol. Neurodegener.* **14,** 1–18 (2019).

18. Greenfest-Allen, E., Cartailler, J.-P., Magnuson, M. A. & Stoeckert, C. J. iterativeWGCNA: iterative refinement to improve module detection from WGCNA co-expression networks. *bioRxiv* 234062 (2017). doi:10.1101/234062

19. Charrad, M., Ghazzali, N., Boiteau, V. & Niknafs, A. **NbClust**: An *R* Package for Determining the Relevant Number of Clusters in a Data Set. *J. Stat. Softw.* **61,** 1–36 (2014).

20. Rousseeuw, P. J. Silhouettes: A graphical aid to the interpretation and validation of cluster analysis. *J. Comput. Appl. Math.* **20,** 53–65 (1987).

21. Clifford, H., Wessely, F., Pendurthi, S. & Emes, R. D. Comparison of Clustering Methods for Investigation of Genome-Wide Methylation Array Data. *Front. Genet.* **2,** 88 (2011).

22. Braak, H., Thal, D. R., Ghebremedhin, E. & Del Tredici, K. Stages of the Pathologic

Process in Alzheimer Disease. *J. Neuropathol. Exp. Neurol.* **70,** 960–969 (2011).

23. Wilson, R. S., Arnold, S. E., Schneider, J. A., Li, Y. & Bennett, D. A. Chronic Distress, Age-Related Neuropathology, and Late-Life Dementia. *Psychosom. Med.* **69,** 47–53 (2007).

24. Mukherjee, S. *et al.* Genetic data and cognitively defined late-onset Alzheimer's disease subgroups. *Mol. Psychiatry* (2018). doi:10.1038/s41380-018-0298-8

25. Ritchie, M. E. *et al.* limma powers differential expression analyses for RNA-sequencing and microarray studies. *Nucleic Acids Res.* **43,** e47–e47 (2015).

26. Yu, G., Wang, L.-G., Han, Y. & He, Q.-Y. clusterProfiler: an R Package for Comparing Biological Themes Among Gene Clusters. *Omi. A J. Integr. Biol.* **16,** 284–287 (2012).

27. Kang, H. M. *et al.* Variance component model to account for sample structure in genome-wide association studies. *Nat. Genet.* **42,** 348–354 (2010).

28. Buniello, A. *et al.* The NHGRI-EBI GWAS Catalog of published genome-wide association studies, targeted arrays and summary statistics 2019. *Nucleic Acids Res.* **47,** D1005–D1012 (2019).

29. McKenzie, A. T. *et al.* Brain Cell Type Specific Gene Expression and Co-expression Network Architectures. *Sci. Rep.* **8,** 8868 (2018).

30. Futch, H. S., Croft, C. L., Truong, V. Q., Krause, E. G. & Golde, T. E. Targeting psychologic stress signaling pathways in Alzheimer's disease. *Mol. Neurodegener.* **12,** 49 (2017).

31. Vogl, T., Gharibyan, A. L. & Morozova-Roche, L. A. Pro-Inflammatory S100A8 and S100A9 Proteins: Self-Assembly into Multifunctional Native and Amyloid Complexes. *Int. J. Mol. Sci.* **13,** 2893 (2012).

32. Horvath, I. *et al.* Pro-inflammatory S100A9 Protein as a Robust Biomarker

552 Differentiating Early Stages of Cognitive Impairment in Alzheimer's Disease. *ACS*
553 *Chem. Neurosci.* **7,** 34–39 (2016).
554 33. White, C. C. *et al.* Identification of genes associated with dissociation of cognitive
555 performance and neuropathological burden: Multistep analysis of genetic, epigenetic,
556 and transcriptional data. *PLOS Med.* **14,** e1002287 (2017).
557 34. Klein, Z. A. *et al.* Loss of TMEM106B Ameliorates Lysosomal and Frontotemporal
558 Dementia-Related Phenotypes in Progranulin-Deficient Mice. *Neuron* **95,** 281–296.e6
559 (2017).
560 35. Gallagher, M. D. *et al.* A Dementia-Associated Risk Variant near TMEM106B Alters
561 Chromatin Architecture and Gene Expression. *Am. J. Hum. Genet.* **101,** 643–663
562 (2017).
563 36. Furney, S. J. *et al.* Genome-wide association with MRI atrophy measures as a
564 quantitative trait locus for Alzheimer's disease. *Mol. Psychiatry* **16,** 1130–8 (2011).
565 37. De Strooper, B. & Karran, E. The Cellular Phase of Alzheimer's Disease. *Cell* **164,**
566 603–615 (2016).
567 38. Lambert, J. C. *et al.* Meta-analysis of 74,046 individuals identifies 11 new
568 susceptibility loci for Alzheimer's disease. *Nat. Genet.* **45,** 1452–1458 (2013).
569 39. Schott, J. M. *et al.* Genetic risk factors for the posterior cortical atrophy variant of
570 Alzheimer's disease. *Alzheimer's Dement.* **12,** 862–871 (2016).
571 40. Kichaev, G. *et al.* Leveraging Polygenic Functional Enrichment to Improve GWAS
572 Power. *Am. J. Hum. Genet.* **104,** 65–75 (2019).
573
574

FIGURES

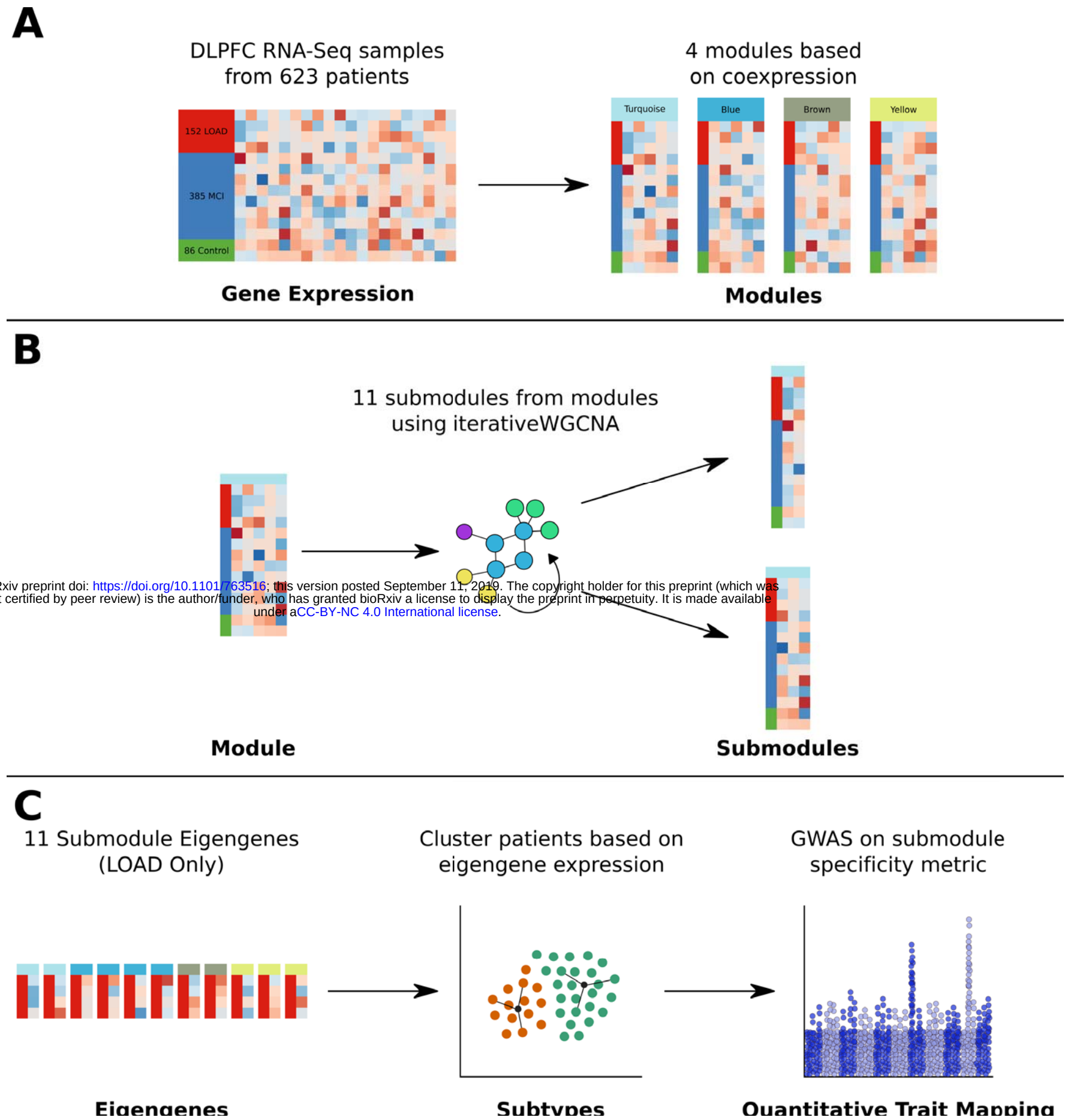

Figure 1: Methodology used in this study to map genetic drivers of LOAD pathology in the ROSMAP cohort. (A) RNA-Seq was performed on dorsolateral prefrontal cortex (DLPFC) tissue from 86 control decedents, 385 decedents with Mild Cognitive Impairment (MCI), and 152 decedents with Late-Onset Alzheimer's Disease (LOAD). A modified procedure using seven different WGCNA protocols, followed by merging by clustering methods, was performed to obtain 4 modules based on gene co-expression. (B) Each of the four modules was subjected to iterativeWGCNA, a procedure that repeatedly performs WGCNA on expression data to generate highly correlated gene sets and exclude weakly correlated genes. 11 submodules were generated from the 4 modules. (C) The eigengene, or first principal component of each submodule, was calculated for all 11 submodules and used as a quantitative trait for single-variant association mapping. Furthermore, the eigengene expression for LOAD cases was used to perform cluster analysis and generate subtypes of LOAD cases. A Euclidean distance quantitative trait was developed to identify genomic loci for each subtype using single-variant association mapping.

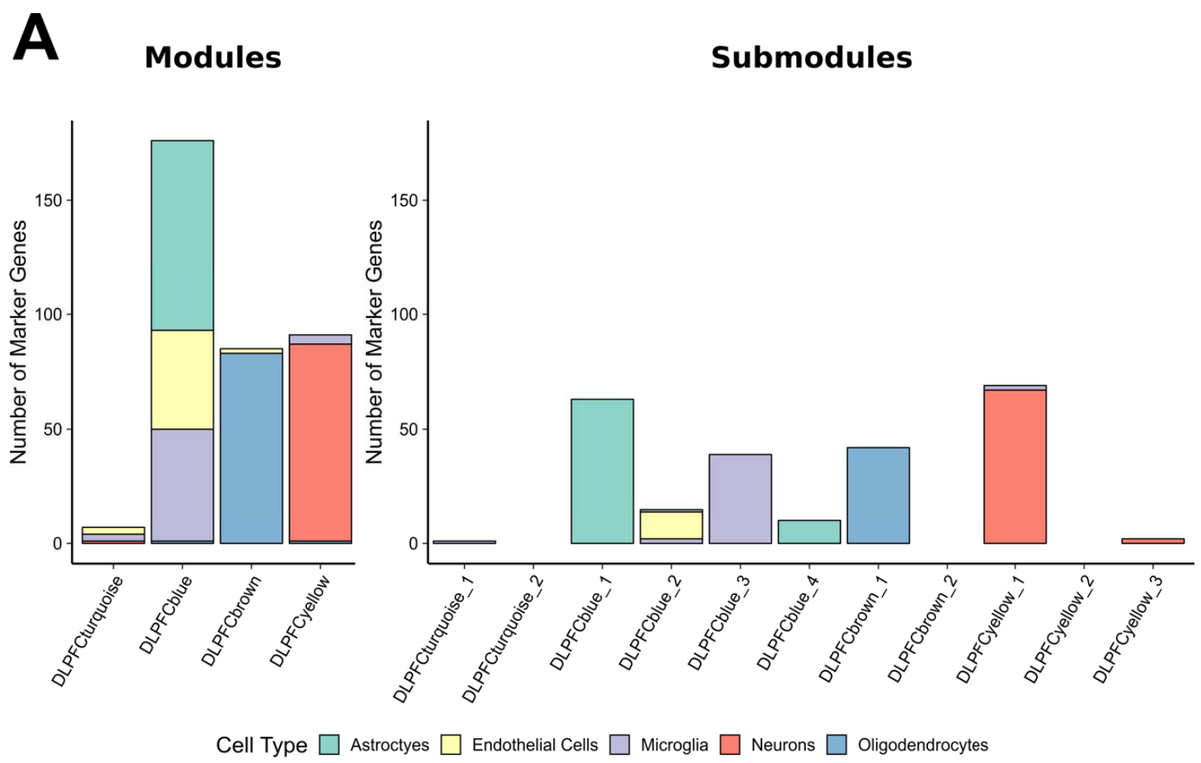

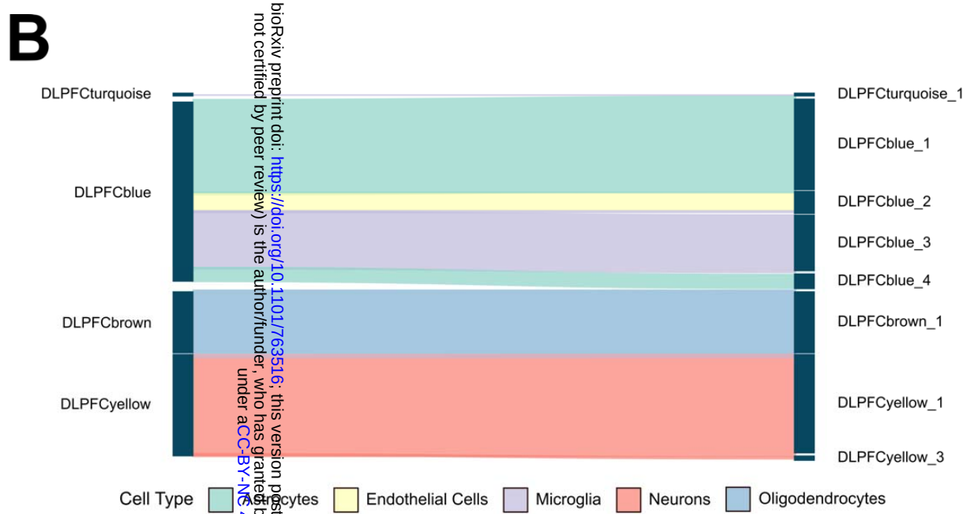

C

DLPFCturquoise_2	Cellular response to heat stress	**DLPFCblue_4**	Regulation of Complement cascade
DLPFCblue_1	Lipid metabolism	**DLPFCbrown_2**	Negative regulation of the PI3K/AKT network
DLPFCblue_2	Signaling by Interleukins	**DLPFCyellow_1**	Neuronal System
DLPFCblue_3	Neutrophil degranulation	**DLPFCyellow_2**	Neuronal System

Figure 2: Cell-type specificity of modules is refined in submodules. (A) Cell type specific marker genes reported by McKenzie *et al.* were used to annotate modules and submodules for astrocytes, endothelial cells, microglia, neurons, and oligodendrocytes. The top 100 marker genes for each cell type were used. The iterativeWGCNA procedure generated submodules that were more cell-type specific than their modules of origin. (B) A Sankey diagram demonstrates which cell-type specific markers from modules were found in submodules generated using iterativeWGCNA for the ROSMAP cohort. (C) Gene set enrichment analysis for Reactome pathways was performed for each submodule gene list. The top enriched Reactome pathways for submodules are reported.

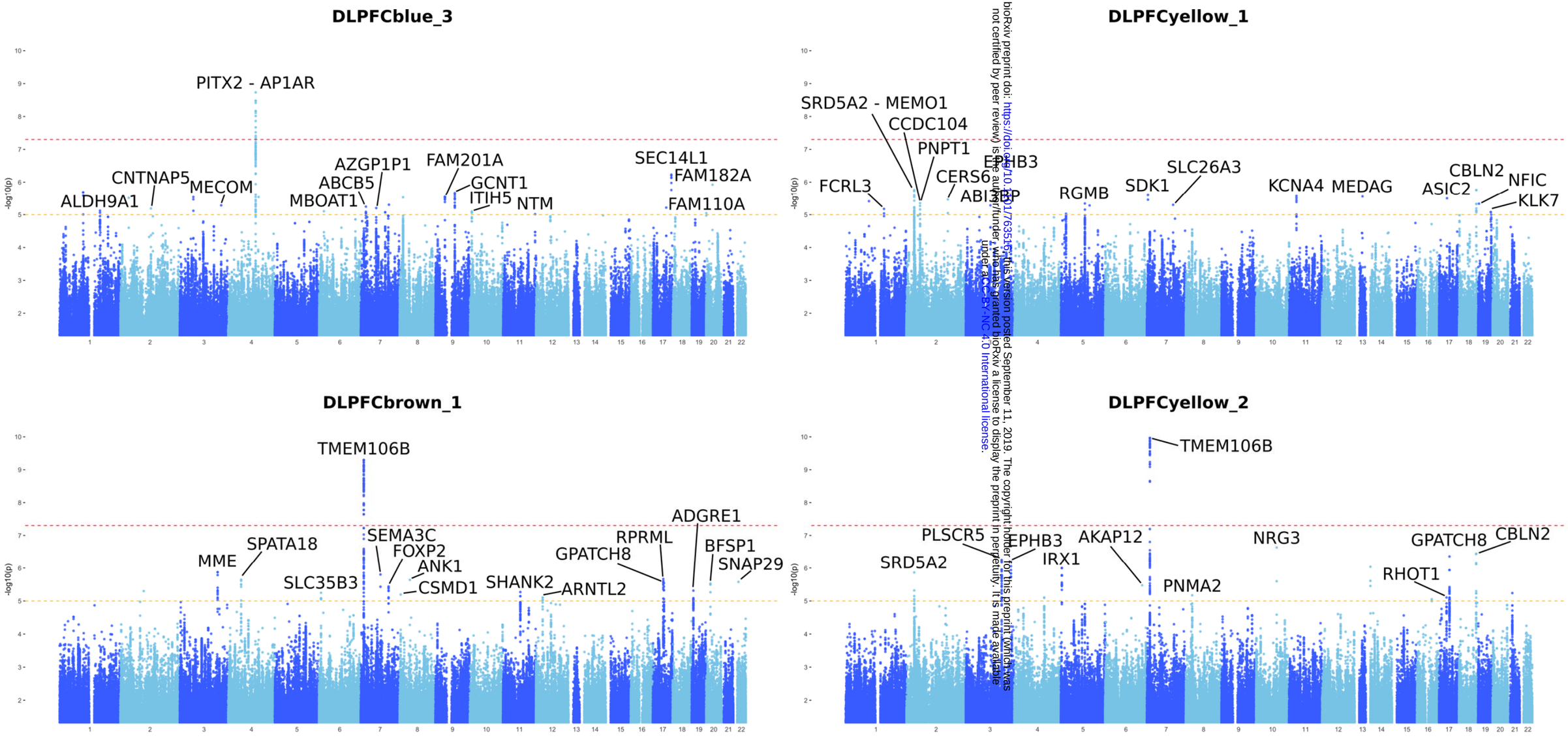

Figure 3: Manhattan plots of single-variant association of select submodule eigengenes in ROSMAP. Eigengene expression for each submodule was used as a quantitative trait when performing single-variant mapping. These Manhattan plots were generated for select DLPFC region submodule eigengenes. Multiple submodule eigengenes were associated with SNPs at a genome-wide significance level of p = 5e-08 (red dotted line). Loci of interest are annotated with the gene closest to the region. Some SNPs were also detected at a genome-wide suggestive level of p = 1e-05 (yellow dotted line). DLPFCblue_3 contains genes related to the TREM2/TYROBP pathway, an important network of genes related to microglial activation during neuroinflammation of the brain. Submodules were associated with both unique and overlapping loci. For example, DLPFCbrown_1 and DLPFCyellow_2 are derived from separate co-expression modules but were both associated with the *TMEM106B* locus. Similarly, DLPFCyellow_1 and DLPFCyellow_2 were derived from the same co-expression module but were associated with a mix of overlapping and unique loci.

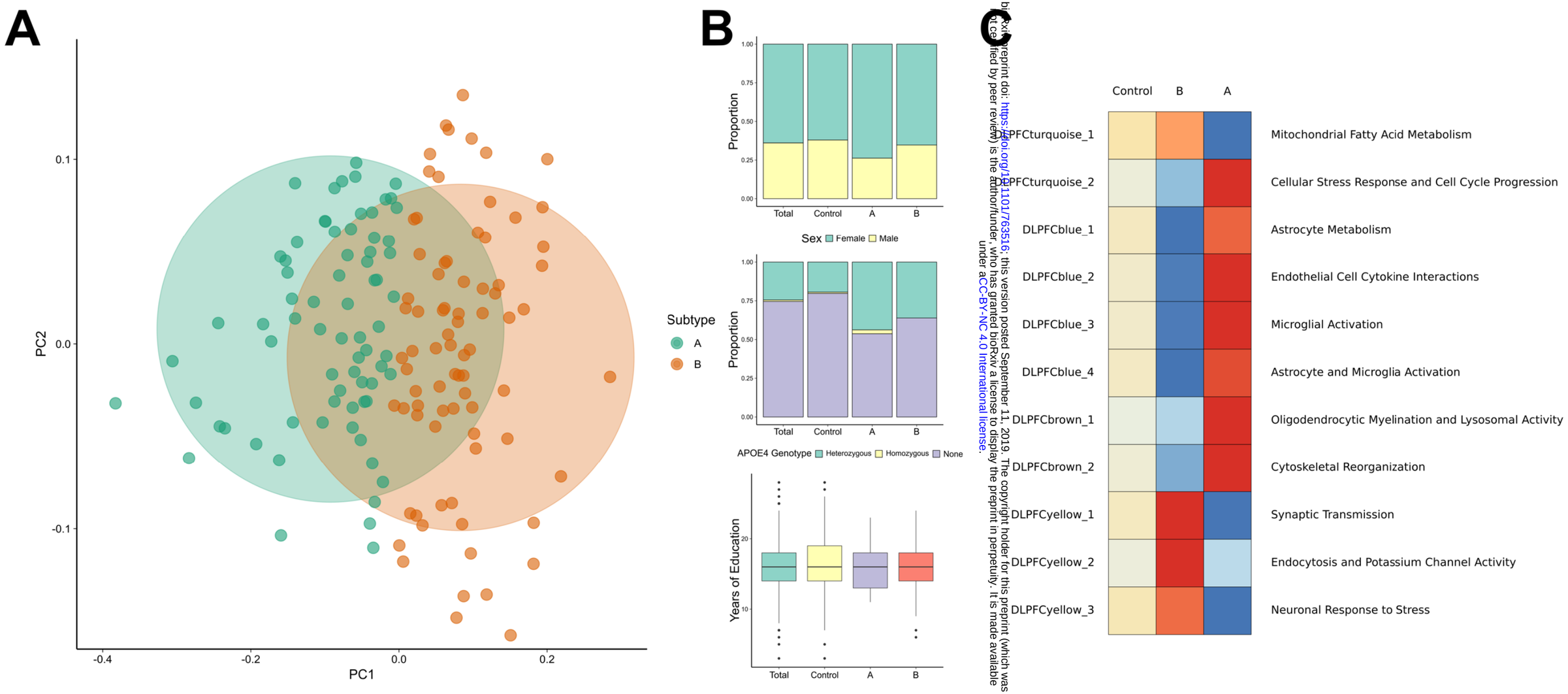

Figure 4: Clustering on eigengene expression in ROSMAP data generates 2 subtypes. (A) Eigengene expression was used to cluster cases into subtypes using K-Means clustering for the DLPFC region. The number of clusters were determined by democratizing results across 30 mathematical indices using the NbClust R package. Two clusters with relatively equal number of cases were generated. (B) There were no significant differences in proportion of sex, *APOEε4* genotype, and years of education between subtypes. (C) The scaled eigengene expression profile of the subtypes demonstrated a strong immune and neuronal signal when compared to control and MCI decedents.

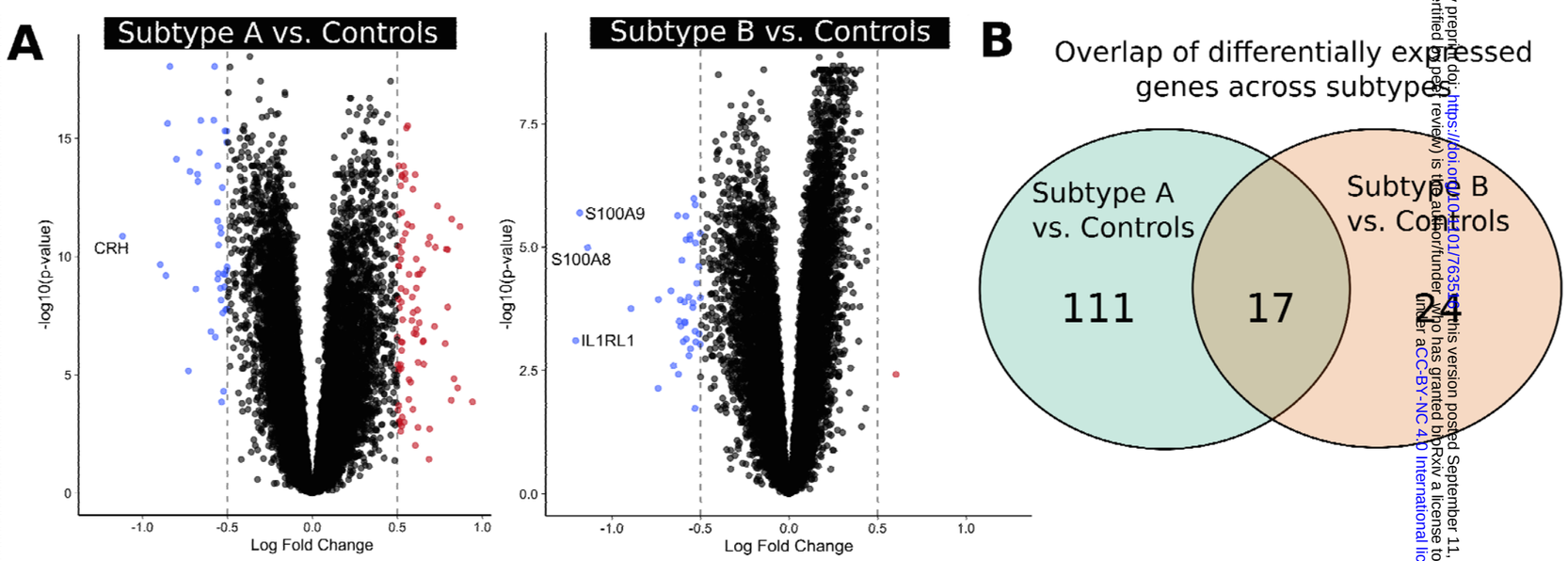

Figure 5: Differential expression analysis of ROSMAP subtypes reveals heterogeneity in inflammatory response in LOAD cases. A) Differential expression analysis comparing each subtype to control decedents for the DLPFC region was performed using the limma R package. We show up-regulated (red, $p < 0.05$, log fold change >0.5) and down-regulated (blue, $p < 0.05$, log fold change < -0.5) genes in the volcano plot and label genes that have an absolute log fold change of greater than 1 (dotted lines). (B) Differentially expressed genes ($p < 0.05$, absolute log fold change > 0.5) from the analysis show a partial overlap between subtypes. (C) Top Reactome pathways for differentially expressed genes for both subtypes are reported. Subtype A demonstrates an enrichment of immune and stress-response related pathways across up-regulated genes, while Subtype B demonstrates a down-regulation of a set of specific immune-related pathways linked to S100A8/A9 activation.

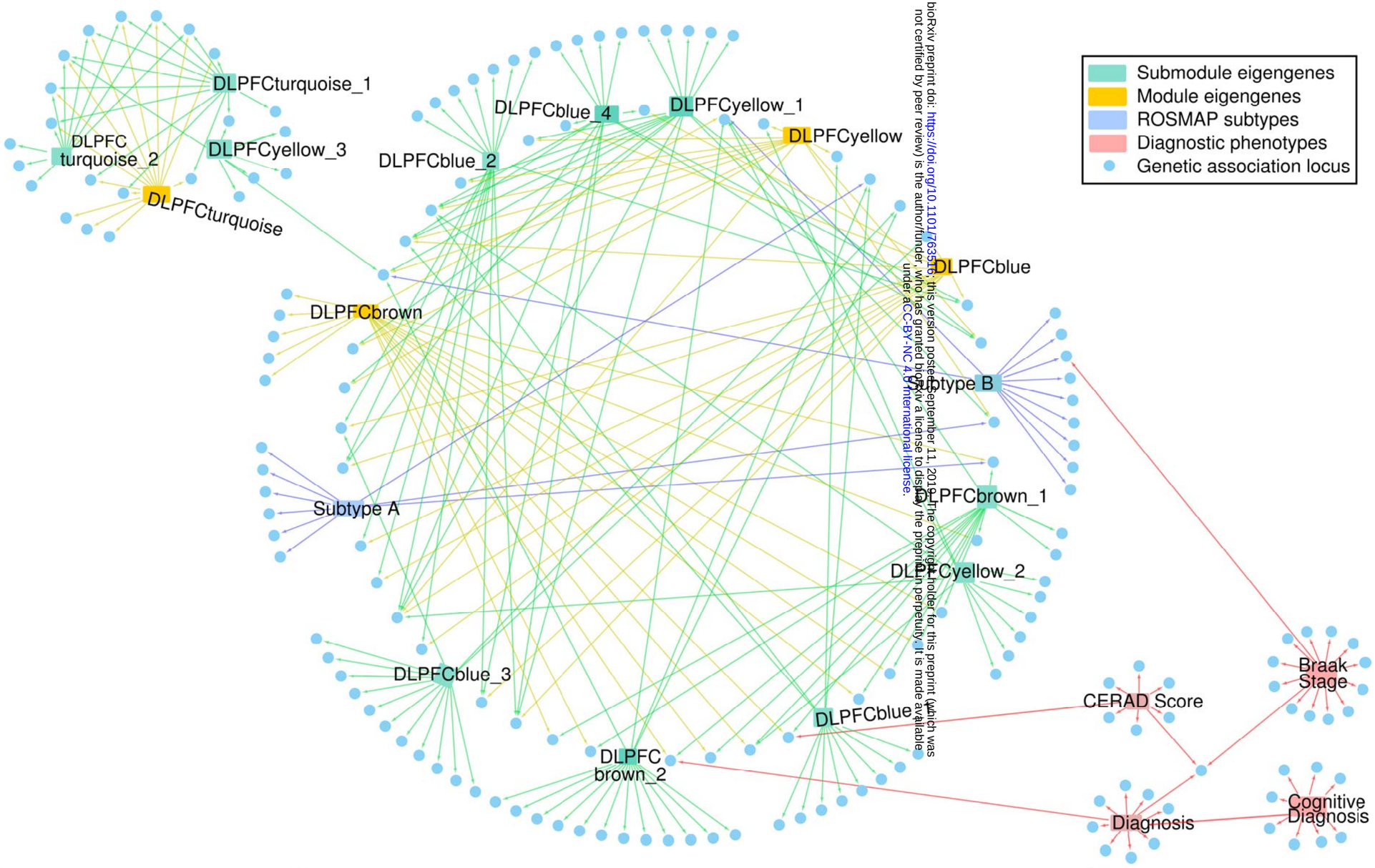

Figure 6: Network of phenotypes and associated loci. We created a directed network describing the loci detected from the multiple analyses in this study. Blue nodes represent loci associated with a phenotype. Red nodes represent phenotypes. An edge from a phenotype to a genetic locus signifies that the locus is associated with the specified phenotype. Diagnostic phenotypes (red edges) were associated with some of the loci detected in this study. The module eigengenes (yellow edges), submodule eigengenes (green edges), and subtypes (blue edges) were associated with overlapping and unique loci (center and left). A community of loci was associated with multiple submodules associated with microglia, endothelial cells, astrocytes, and oligodendrocytes (center). A small community of loci was associated with submodules related to proteostasis (left). Diagnostic phenotypes included CERAD scores, Braak stages, cognitive diagnosis, and case-control association.